







Cite this: DOI: 10.1039/
d6md00096g

Light-controlled inhibition of Gram-positive bacteria by photoswitchable amphiphilic lipids (PALs)

Guilherme F. S. Fernandes, ^{†‡}^a Seong-Heun Kim, [†]^b Charlotte K. Hind,^c Jessica Furner-Pardoe,^c Janis Romanopulos, ^b Christian D. Lorenz, ^d A. James Mason, ^b J. Mark Sutton^c and Daniele Castagnolo ^{*a}

Amphiphilic lipids are potent membrane-disrupting antibacterials, but their activity cannot normally be modulated after administration. Here we report photoswitchable amphiphilic lipids (PALs) that enable reversible, light-controlled modulation of antibacterial potency through photoinduced changes in molecular conformation. The PALs incorporate azobenzene photoswitches linking quaternary ammonium headgroups to variable alkyl chains, allowing their geometry and membrane affinity to be tuned by *trans-cis* isomerisation. Systematic studies against multidrug-resistant Gram-positive bacteria revealed a striking, chain-length-dependent photomodulation. Short-chain PALs lost activity upon irradiation, whereas long-chain derivatives became strongly antibacterial in their *cis*-enriched states, with up to 32-fold reductions in MICs. Molecular dynamics simulations correlated these changes with light-dependent differences in membrane insertion depth and molecular orientation, providing a structural basis for optical control of membrane disruption. These findings establish a mechanistic framework for designing photoswitchable amphiphiles that translate molecular photoisomerisation into controllable biological function, extending the reach of photopharmacology into antibacterial membrane-active agents.

Received 5th February 2026,
Accepted 23rd April 2026

DOI: 10.1039/d6md00096g

rsc.li/medchem

Introduction

Cell membranes are essential for bacterial viability, serving as dynamic platforms for metabolism, nutrient transport, and homeostatic regulation.^{1–3} Owing to their central role, they have emerged as compelling targets for the development of next-generation antibacterial agents.^{4,5} Among the most promising classes of membrane-damaging molecules are cationic amphiphiles, which exhibit potent antibacterial activity through membrane disruption.^{6–8} Although their precise mechanisms of action remain only partially elucidated, it is widely accepted that these molecules penetrate the bacterial cell wall and interact with membrane lipids and proteins, leading to structural disorganization,

leakage of cytoplasmic contents, and degradation of intracellular components.^{1,4,5,9,10} Structurally, cationic amphiphiles typically contain at least one positively charged headgroup, such as a quaternary ammonium cation (QAC) or a guanidinium moiety, that electrostatically associates with the negatively charged phospholipids of bacterial membranes (Fig. 1a). Concurrently, their hydrophobic structural components intercalate into the membrane core, increasing surface pressure and inducing a transition toward a liquid-crystalline state. This process perturbs membrane integrity, alters osmoregulatory balance, and reduces the hydrophobic barrier of the lipid bilayer, ultimately compromising cell viability.^{10–12}

Photopharmacology has recently emerged as a strategy to modulate drug conformation, activity, and selectivity using light-responsive photoswitches.^{13–15} Azobenzenes are particularly attractive photoswitches due to their efficient and reversible *trans-cis* isomerization upon light irradiation.^{16–18} Azobenzene-containing compounds have been applied in antitumor therapies,^{19–21} ion channels,^{22,23} HDACs,^{24,25} kinases,^{26,27} and antibacterials.^{18,28} Despite notable examples, such as the azobenzene–quinolone conjugate **4** that displays enhanced antibacterial activity against *E. coli*²⁹ and the carbohydrate–azobenzene surfactant **5** capable of controlling biofilm growth (Fig. 1b),³⁰ the development of

^a Department of Chemistry, University College London, 20 Gordon Street, London WC1H 0AJ, UK. E-mail: d.castagnolo@ucl.ac.uk^b Institute of Pharmaceutical Science, School of Cancer & Pharmaceutical Science, King's College London, 150 Stamford Street, SE1 9NH, London, UK^c Antimicrobial Discovery, Development and Diagnostics, Vaccine Development and Evaluation Centre, UKHSA Porton Down, Salisbury SP4 0JG, UK^d Biological Physics and Soft Matter Group, Department of Physics, King's College London, London WC2R 2LS, UK[†] These authors contributed equally.[‡] Present Address: Chemical Biology Science Technology Platform, The Francis Crick Institute, London, NW1 1AT, UK.

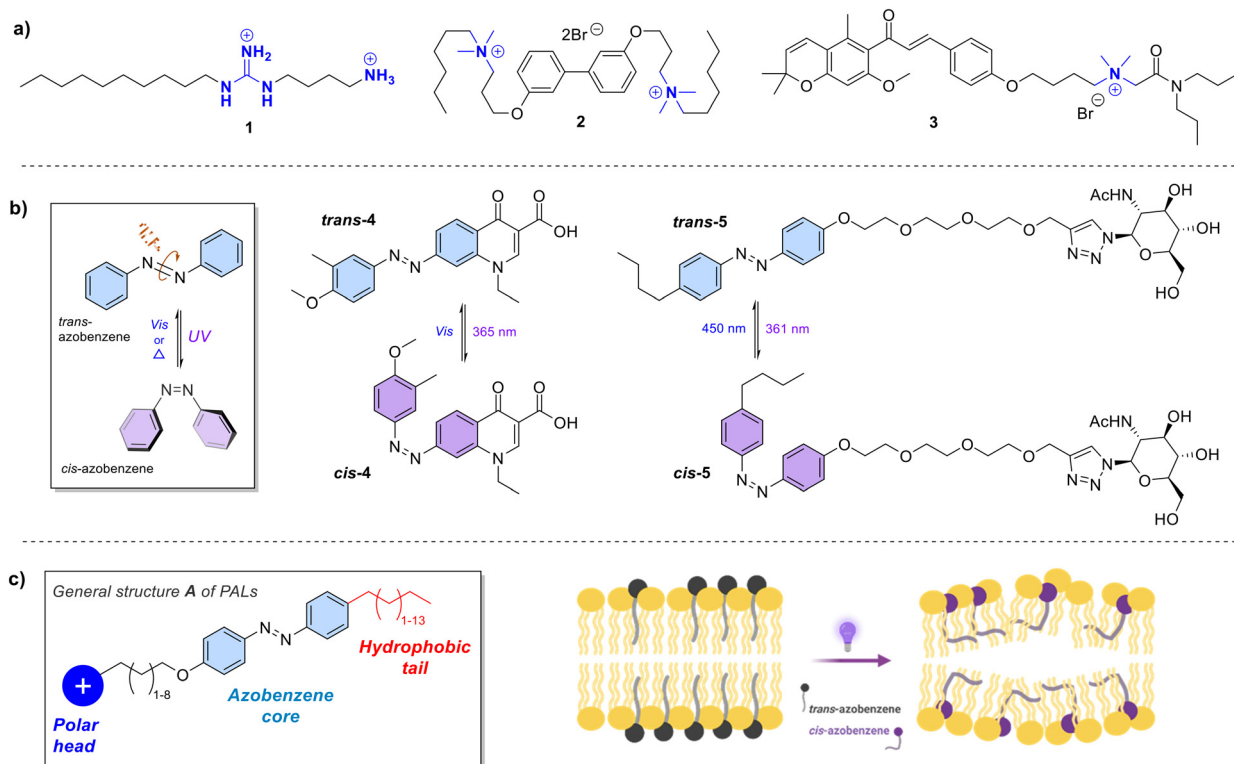


Fig. 1 a) Cationic amphiphile antibacterials; b) azobenzenes with antibacterial activity; c) general structure of photoswitchable amphiphilic lipids (PALs) and their putative interaction with bacterial membranes. Created with <https://www.BioRender.com>.

photoswitchable antibacterials still remains limited. However, azobenzene-based photoswitchable antimicrobials still hold significant potential for localized therapeutic applications. Since the photoisomerisation of azobenzene derivatives is typically triggered by UV or blue light, which have limited tissue penetration, these systems are particularly well suited for topical or surface-associated treatments.

Potential scenarios include light-directed treatment of superficial infections such as wounds, as well as catheter- or implant-associated infections, where controlled illumination can be applied at the infection site. In addition, PALs could be envisioned as photoresponsive coatings for medical surfaces, enabling spatial and temporal control of antibacterial activity.

Building on our broader interest in membrane-interacting antibacterial agents such as lipoguanidines and in bacterial membranes as dynamic therapeutic targets,⁶ here we explore how light can be harnessed to modulate the interactions between bacterial membrane and lipid-based antibacterials in a controllable manner.

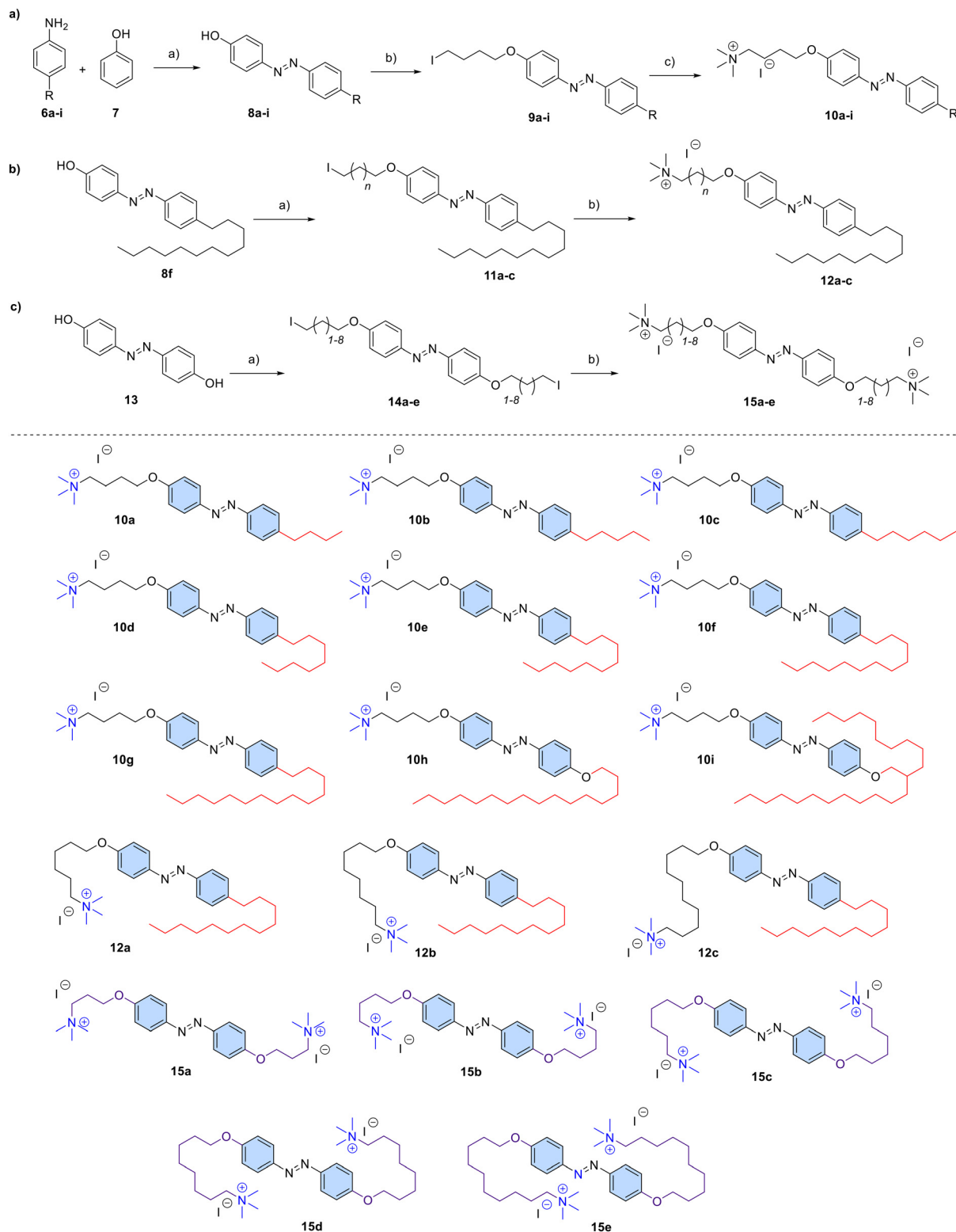
We designed and synthesized a new class of photoswitchable amphiphilic lipids (PALs) that combine the membrane-interacting features of amphiphilic molecules with the reversible conformational control of molecular photoswitches (general structure A, Fig. 1c). These PALs incorporate one or two quaternary ammonium (QAC) headgroups connected through an azobenzene unit to hydrophobic *n*-alkyl tails of variable lengths. We hypothesize

that light-induced *trans*–*cis* isomerization of the azobenzene core will alter the molecular conformation and packing of the PALs at the membrane interface, thereby modulating their ability to insert into and potentially disrupt bacterial membranes. This approach provides a mechanistic framework for developing light-responsive, membrane-targeting antibacterials whose activity can be precisely tuned through external optical stimuli. Here we demonstrate that light-driven conformational control can switch antibacterial activity on or off depending on the amphiphile chain length, establishing a direct link between molecular geometry and membrane disruption efficiency.

Results and discussion

A library of PALs was designed and synthesized as reported in Scheme 1. PALs **10a–i**, presenting different hydrophobic alkyl chains while keeping the cationic ammonium group at four carbon unit distance from the azobenzene switch, were first synthesized. The azobenzene motifs **8a–i** were obtained through an azo coupling reaction between appropriate anilines **6a–i** and phenol **7**. Subsequently, the derivatives **8a–i** underwent alkylation with 1,4-diiodobutane *via* an $\text{S}_{\text{N}}2$ reaction, resulting in alkylated intermediates **9a–i**. Finally, the quaternary ammonium cation was inserted through nucleophilic substitution of iodines with trimethylamine, leading to the formation of the positively charged PALs **10a–i**.





Scheme 1 First series of photoswitchable amphiphilic lipids. Conditions: a) NaNO_2 , NaOH , Na_2CO_3 , HCl , H_2O , acetone, $0^\circ\text{C} > \text{RT}$, 3 h, 22–69%; b) 1,4-diiodobutane, Cs_2CO_3 , acetone, 80°C , 1 h, 46–83%; c) trimethylamine, THF, 75°C , 1 h, 90–99%.

A second series of derivatives **12a–c** having the same aliphatic hydrophobic chain as **10f** and the polar ammonium cation at different distances from the azobenzene switch, was then synthesized (Scheme 1b). The

intermediate **8f** was alkylated with appropriate diiodoalkanes to provide the iodo-derivatives **11a–c**, which were in turn converted into the PALs **12a–c** through reaction with Me_3N .



Finally, a series of PAL derivatives presenting two QAC moieties (Scheme 1c) was prepared. Five bis-QAC-azobenzenes **15a–e** were designed, featuring diverse carbon chain lengths connecting the azobenzene core and the polar QAC heads.

The phenol derivative **13** was first reacted with 2 equivalents of the appropriate diiodoalkanes to give the diiodo-derivatives **14a–e**. The latter were finally converted into the bis-QAC-azobenzenes **15a–e** through reaction with Me_3N .

The photoisomerization properties of the PAL compounds were then characterized by UV-vis spectroscopy. Representative spectra for compounds **10b** and **10f**, which were later found to exhibit opposite trends in the microbiological assays, as well as for the bi-cationic compound **15c** are shown in Fig. 2. UV-vis spectroscopic data for other compounds are available in the SI (Fig. S8–S13). PALs **10b** and **10f** were first irradiated in CH_3CN with 365 nm UV light for 1.5 hours at 37 °C, to replicate the antibacterial assay conditions. Following UV-vis irradiation, the spectra exhibited a characteristic $\pi \rightarrow \pi^*$ transition band for the *trans*-isomers with maximum intensity at *ca.* 350 nm and a characteristic $n \rightarrow \pi^*$ transition band for their *cis*-isomers with a maximum at *ca.* 440 nm. After UV irradiation, **10b** and **10f** were left for 24 hours in darkness at 37 °C resulting in

the photorelaxation of *cis*-isomers back to *trans*-isomers (Fig. 2a and b). The photorelaxation initiates approximately 4 hours after the UV irradiation was stopped, culminating in the peak *trans*-form after 24 hours. The *trans*-to-*cis* isomerization and the *cis*-to-*trans* photorelaxation of **10b** and **10f** were also confirmed by ^1H NMR analysis in $\text{DMSO-}d_6$ solution (Fig. 2d and e). Notably, under dark conditions, PALs exist as thermally stable *trans*-isomers (*trans*-dominated photostationary state (PSS): 89–96%) when freshly prepared. Following irradiation with 365 nm UV light in dark-adapted conditions at 37 °C for 1 hour, the *trans*-isomers efficiently transitioned into *cis*-isomers (*cis*-dominated photostationary state (PSS): 89–94%). Then, when the light was switched off and the PALs were left 6 hours in dark-adapted conditions at 37 °C, the ratio between *trans*- and *cis*-PSS of PALs adjusted at 60% and 40% respectively after 6 hours.

Furthermore, photoisomerization studies in TSB bacterial growth media were carried out to examine the azobenzenes' photoisomerization properties in the media used in antibacterial assays (Fig. S6 and S7). Remarkably, the UV-vis spectra in TSB media displayed analogous transition band characteristics to those observed in CH_3CN solution. A similar photoisomerization and photorelaxation behaviour was observed for all PALs **10** and **12**. Interestingly, no

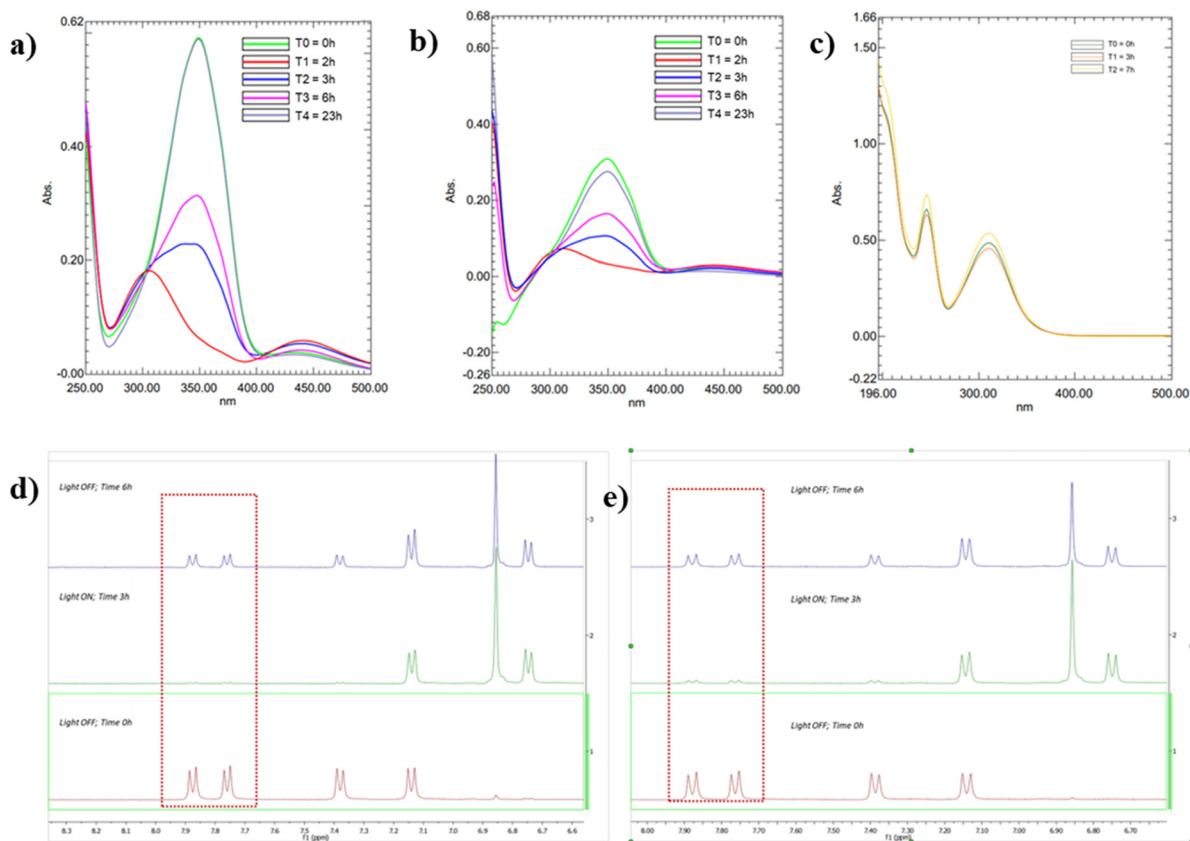


Fig. 2 UV-vis spectrophotometric analysis of a) compound **10b** and b) compound **10f**, showing *trans*-to-*cis* isomerization and *cis*-to-*trans* photorelaxation; c) UV-vis spectrophotometric analysis of the bi-cationic PAL **15c** showing no *trans*-to-*cis* isomerization upon 365 nm UV light irradiation; NMR analysis of the photoisomerization of d) **10b** and e) **10f**, showing the shifting of the aromatic signals due to *trans*-to-*cis* isomerization upon 365 nm UV light irradiation and *cis*-to-*trans* photorelaxation in the dark.



trans-to-*cis* isomerization was observed for the bi-cationic compounds **15**, as shown in Fig. 2c for **15c** when irradiated with 365 nm UV light.

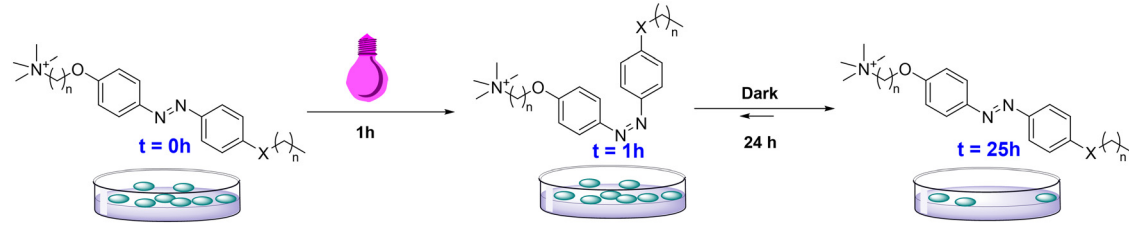
The antibacterial efficacy of PALs **10a–i**, **12a–c** and **15a–e** against a panel of drug-sensitive and MDR Gram-positive bacterial strains (*S. aureus* MSSA ATCC 9144, MRSA NCTC 13616, MRSA USA 300, and MRSA SA 1199B; *E. faecalis* VSE NCTC 775 and VRE NCTC 12201; *E. faecium* VRE NCTC 12204) was then assessed through an OD₆₀₀ bacterial growth assay (see SI for experimental details).⁶ Two parallel sets of experiments were carried out. First, bacteria were incubated with each PAL in their native relaxed *trans*-PSS under dark conditions at 37 °C (Table 1, light OFF (LOFF) experiments). Secondly, to induce photoisomerization to *cis*-enriched PSS, microplates containing bacteria and PALs were exposed to 365 nm UV light for 1 hour under incubation conditions. After this light-on period, the plates were kept in the dark for a further 24-hour incubation at 37 °C (Table 1, light ON (LON) experiments). Importantly, a control experiment involving only bacteria and UV irradiation was carried out, demonstrating the non-toxic nature of the 365 nm UV light on bacteria. The minimum inhibitory concentration (MIC) was employed to evaluate antibacterial activity (Table 1).

The majority of PALs demonstrated good micromolar activity against all seven tested Gram-positive bacterial

strains, underscoring both potency and broad-spectrum efficacy. Notably, a distinct photomodulation of the antibacterial activity was observed across various compounds. Compounds **10a–c** bearing short alkyl chains (4 to 6 carbons) exhibited a substantial loss of potency against all tested strains following UV light irradiation, resulting in an increase in MIC values, from 2–4 µg mL⁻¹ to 16–32 µg mL⁻¹ (Table 1, entries 1–3). The antibacterial activity of PAL **10a**, also known as AzoTAB, against *S. aureus* under LOFF conditions is in agreement with that previously described.^{30–32} However, while in previous reports no difference in the antibacterial activity of **10a** in both the *cis*-PSS and the *trans*-PSS was observed, we found an increase in the MIC values against all the four strains of *S. aureus* following photoirradiation. Such variation in results can be attributed to different conditions employed for the bacterial assay, such as 5 minutes of irradiation of **10a** before incubation with bacteria,³⁰ versus the exposure of **10a** to UV light for 1 hour during incubation in our assay. It is plausible that the different exposure time to UV light may determine a different *cis*-PSS/*trans*-PSS ratio or a faster *cis*-to-*trans* relaxation and that the presence of higher amount of *cis*-PSS in our assay may be responsible for the observed increased MICs.

Compounds **10f–h** bearing carbon chains spanning 10–14 carbons, displayed an increased potency against the Gram-

Table 1 Light control of antibacterial activity in photoswitchable amphiphilic lipids (PALs) against Gram-positive bacteria^a



Entry	Cmpd	MIC (µg mL ⁻¹)													
		<i>S. aureus</i>				<i>E. faecalis</i>				<i>E. faecium</i>					
		MSSA ATCC 9144		MRSA NCTC 13616		MRSA USA 300		MRSA SA 1199B		VSE NCTC 775		VRE NCTC 12201		VRE NCTC 12204	
LOFF	LON	LOFF	LON	LOFF	LON	LOFF	LON	LOFF	LON	LOFF	LON	LOFF	LON		
1	10a	2	8	4	16	2	16	4	16	2	16	8	16	8	16
2	10b	2	8	4	16	2	16	4	32	4	16	4	32	2	32
3	10c	4	4	4	8	2	8	4	16	2	8	4	16	2	16
4	10d	4	4	8	4	4	4	4	4	4	4	4	4	4	4
5	10e	16	2	16	2	16	4	>128	4	4	2	16	2	4	2
6	10f	>128	8	>128	8	>128	4	>128	4	>128	4	>128	4	>128	4
7	10g	>128	16	>128	8	>128	16	>128	8	>128	8	>128	16	>128	16
8	10h	>128	16	>128	2	>128	>128	>128	>128	>128	>128	>128	>128	>128	>128
9	10i	>128	>128	>128	>128	>128	>128	>128	>128	>128	>128	>128	>128	>128	>128
10	12a	>128	ND	>128	4	>128	4	>128	8	>128	4	>128	8	>128	8
11	12b	>128	32	>128	16	>128	16	>128	32	>128	16	>128	32	>128	8
12	12c	>128	>128	>128	>128	>128	>128	>128	>128	>128	>128	>128	>128	>128	>128
13	15a	>128	>128	>128	>128	>128	>128	>128	>128	>128	>128	>128	>128	>128	>128
14	15b	>128	>128	>128	>128	>128	>128	>128	>128	>128	>128	>128	>128	>128	>128
15	15c	>128	>128	>128	>128	>128	>128	>128	>128	>128	>128	>128	>128	>128	>128
16	15d	128	64	>128	128	128	128	>128	>128	>128	>128	>128	>128	128	>128
17	15e	16	8–16	64	16	32	16–32	64	32	32	16–32	64	32–64	64	32

^a Color coding: red, ≥3–4-fold increase in MIC after UV irradiation; green, ≥4-fold reduction in MIC.



positive panel when irradiated with UV-light (Table 1, entries 6–8). Compounds **10f** and **10g**, characterized by 12 and 14 carbons in the alkyl tail, showed no antibacterial activity against all the Gram-positive strains ($\text{MIC} = \geq 128 \mu\text{g mL}^{-1}$) when in *trans*-PSS respectively, while a remarkable decrease in the MICs (up to $4 \mu\text{g mL}^{-1}$) was observed upon UV irradiation ($\text{MIC reduction} > 32$ fold). Interestingly, PALs **10d** and **10e**, bearing respectively medium-length 8 and 10 carbon chains, showed good activity against all Gram-positive strains, and no differences in MIC between the *trans*-PSS and the *cis*-PSS (Table 1, entries 4–5). Compound **10d** was the sole PAL maintaining the same antibacterial activity in both *trans* and *cis* isomeric forms ($\text{MIC} = 4\text{--}8 \mu\text{g mL}^{-1}$), while compound **10e** showed moderate MIC decrease upon UV irradiation on MSSA ATCC 9144 and MRSA NCTC 13616 strains, and a remarkable increase of activity ($\text{MIC} = 4 \mu\text{g mL}^{-1}$) on MRSA SA 1199B upon UV light irradiation (entry 5). Interestingly, PAL **10h**, featuring a 16-carbon alkyl tail, was inactive against all tested Gram-positive strains in both *trans*- and *cis*-PSS, with the exceptions against the MSSA ATCC 9144 and MRSA NCTC 13616 strains, where it exhibited a noteworthy reduction in MIC of 8–64-fold, respectively. Finally, PAL **10i**, bearing a double alkyl tail comprising 10 and 12 carbon atoms did not show any activity in either isomeric form, with $\text{MIC} > 128 \mu\text{g mL}^{-1}$. A clear structure–activity pattern is evident for PALs **10a–i**, with shorter chain PALs exhibiting an increase of MIC values upon UV irradiation while a decrease of MICs was observed for PALs with longer chains. PALs **12a–c**, bearing different alkyl linkers between the azobenzene photoswitch and the QAC unit, showed a similar trend confirming the linear correlation between the length of the PAL alkyl chains and the antibacterial activity. As the carbon chain lengthened, PALs **12a–c** showed no activity on the *trans*-PSS, while, following photoisomerization upon UV irradiation, they displayed a significant reduction in MICs ($4\text{--}32 \mu\text{g mL}^{-1}$, Table 1, entries 10–11). On the other hand, PAL **12c**, characterized by a 10-carbon long chain, exhibited no antibacterial activity either in the *cis*-PSS or the *trans*-PSS (Table 1, entry 12). It is evident that an ideal length of the PAL is required to have an antibacterial activity in the *trans*-PSS (LOFF experiments), Fig. 3.

Previous studies on QAC derivatives clearly showed a correlation between the antibacterial activity and the length of their alkyl tails, with the most effective QAC compounds containing seven to twelve carbon atoms.^{33,34} This behaviour is consistent with the known “cutoff effect” in amphiphilic systems, where activity initially increases with alkyl chain elongation up to an optimal length and then sharply declines due to reduced solubility or membrane partitioning.^{35–39} Interestingly, UV-induced isomerization appears to reverse this inactivity for long-chain PALs, restoring antibacterial efficacy in compounds that are otherwise inactive in their *trans* forms. This finding suggests that photoisomerization can modulate the balance between hydrophobicity and solubility, enabling antibacterial activity even beyond the conventional cutoff length.

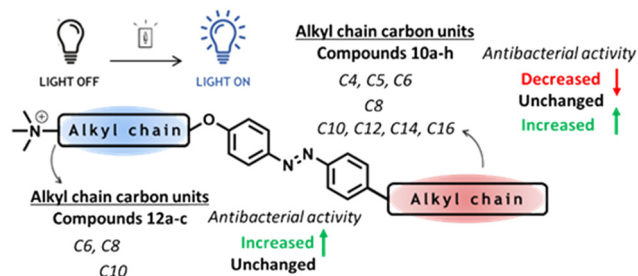


Fig. 3 Summary of the structure–activity relationships (SAR) of antimicrobial compounds **10a–h** and **12a–c**, highlighting the effect of alkyl chain length on minimum inhibitory concentration (MIC) under light-activated conditions. For compounds **10a–c** bearing shorter alkyl chains (C4–C6) an increase of MIC values was observed following UV irradiation, while compounds **10e–h** bearing longer chains (C10–C16) showed an improved activity (decreased MIC) after UV irradiation. Compound **10d** with C8 chain showed no variation in MIC. In contrast, for compound series **12a–c**, shorter chains (C6–C8) are associated with increased potency (reduced MIC), whereas C10 shows no significant variation.

Finally, PALs **15a–e**, bearing two QACs on each end of the azobenzene core, did not show any antibacterial activity before and after UV light irradiation (Table 1, entries 13–17). Since compounds **15a–e** are not subject to *trans*-to-*cis* isomerization, and they remain in the *trans*-enriched PSS upon UV irradiation, no differences are observed in the MIC under both LOFF or LON experiments.

All the synthesized PALs were also assayed against a panel of Gram-negative bacteria (*K. pneumoniae* NCTC 13368 and M6; *A. baumannii* AYE and ATCC 17978; *P. aeruginosa* PAO1 and NCTC 13437; and *E. coli* NCTC 12923) under LOFF and LON conditions. In all cases, no antibacterial effect was observed, with MIC values consistently $> 64 \mu\text{g mL}^{-1}$ across the studied microorganisms (Table S1). This behaviour can be rationalised by the presence of the LPS-rich outer membrane of Gram-negative bacteria, which limits the penetration of cationic amphiphiles. Short-chain PALs likely lack sufficient hydrophobicity to traverse this barrier, whereas longer-chain derivatives and bis-quaternary ammonium compounds (**15a–e**), due to their increased hydrophobicity, charge density, and steric bulk, may be preferentially retained at the membrane surface rather than efficiently translocating across it.

The observed reversal of antibacterial activity upon photoisomerization, particularly in long-chain PALs, suggests that molecular conformation may play a crucial role in modulating membrane interactions. To probe this hypothesis, we conducted molecular dynamics (MD) simulations on representative short- and long-chain derivatives, **10b** and **10f**, to examine how photoinduced isomerisation affects their structural behaviour and interaction with a model Gram-positive membrane (Fig. 4).

Analysis of C–N=N–C dihedral angles and the fraction of these dihedrals in the *cis* conformation across both single- and mixed-conformer systems revealed that both compounds largely retained their initial conformations



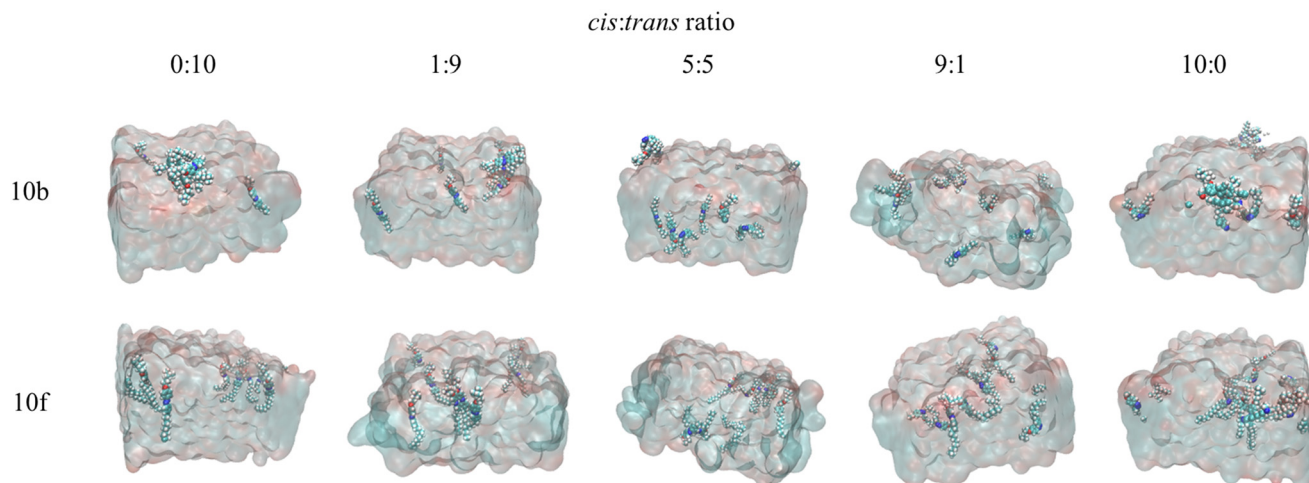


Fig. 4 Snapshot of 10 compounds interacting with a model Gram-positive membrane (POPG) during molecular dynamics (MD) simulations. Compounds are shown in vdW representation; membrane is shown in QuickSurf representation. All snapshots were taken at 175 ns, except for compound **10f** at a 5:5 *cis*:*trans* ratio, which was taken at 140 ns.

throughout the simulation. In single-conformer systems, *cis* conformers consistently exhibited dihedral angles near 0° , while *trans* conformers remained clustered around $\pm 180^\circ$, indicating high conformational stability.⁴⁰

This trend persisted across all *cis*:*trans* ratios in mixed-conformer systems, with each conformer maintaining its characteristic dihedral angle distribution. Notably, *cis* conformers displayed slightly broader dihedral angle distributions and greater variability in *cis* fraction, particularly at higher *cis* content, suggesting increased conformational flexibility within the membrane environment.⁴¹

Compound **10f** consistently demonstrated increased membrane insertion in comparison to compound **10b** across all simulations (Fig. 5). The membrane insertion profiles reveal bimodal distributions for both compounds, indicating two distinct molecular populations: inserted into the hydrophobic tails of the lipid membrane (positive insertion depths) and non-inserted (negative insertion depths). Those with negative insertion depths may be interacting with the lipid headgroups.⁴² In single-conformer systems, for compound **10b**, the majority population exhibited mean insertion depths of -9.7 Å (*cis*, 80%) and -9.8 Å (*trans*, 80%), indicating that most of the molecules remained outside the hydrophobic core of the membrane. However, a minor population showed membrane insertion with depths of 8.5 Å (*cis*, 20%) and 9.7 Å (*trans*, 20%). In contrast, compound **10f** showed significantly enhanced insertion with the majority of the molecules successfully embedded within the membrane. The predominant population showed deeper insertion depths of 11.2 Å (*cis*, 71%) and 8.5 Å (*trans*, 89%), while the minority population remained outside the membrane at -11.3 Å (*cis*, 29%) and -8.7 Å (*trans*, 11%). This represents a fundamental difference in membrane affinity between the two compounds.⁴³

Mixed conformer systems reinforced this trend across varying *cis*:*trans* ratios (1:9, 5:5, 9:1). Compound **10f**

consistently maintained higher proportions of inserted molecules and achieved greater insertion depths across all ratios. Interestingly, compound **10f** at the 5:5 ratio showed reduced inserted population (44–45%) compared to the other ratios, suggesting that the ratio of the conformers present in solution may influence membrane insertion efficiency.

These trends were further supported by simulations of mixed *cis*:*trans* conformer ratios.

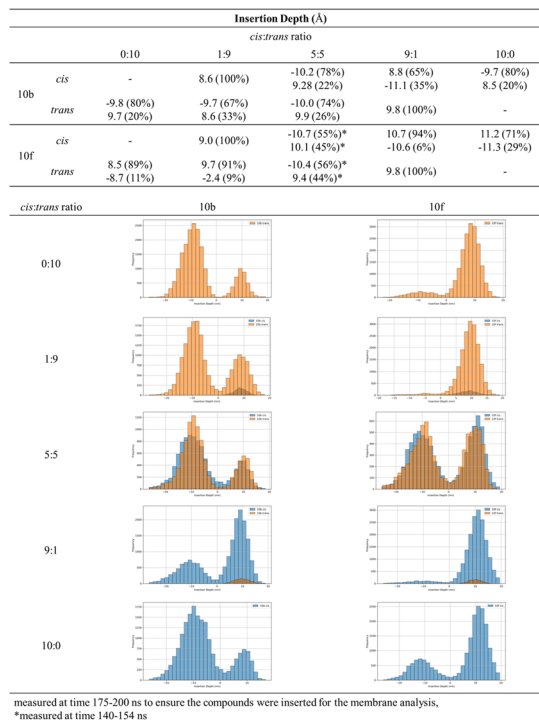
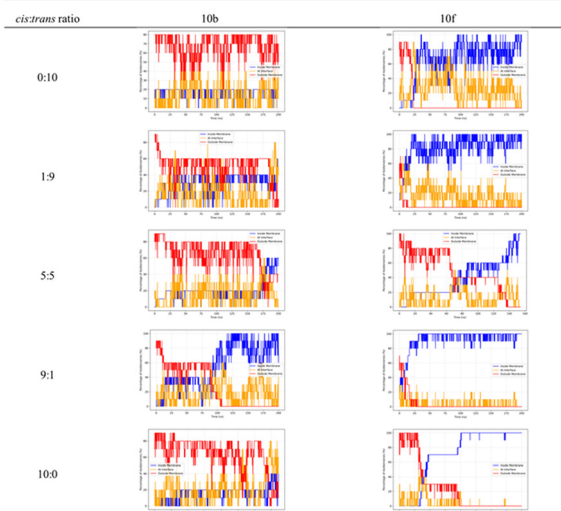


Fig. 5 Membrane insertion profiles of compound **10b** and **10f** across varying *cis*:*trans* conformer ratios. Histograms demonstrate bimodal distributions with inserted (positive depths) and non-inserted (negative depths) indicating population distribution.



Compound **10b** was frequently found to remain in the aqueous or interfacial regions of the simulated systems during the simulations. Compound **10f** demonstrated rapid and sustained membrane insertion, with molecules quickly achieving stable positions within the lipid bilayer core across most conformer ratios (Fig. 6). Compound **10b** exhibited limited and variable insertion depending on the conformer ratio (Fig. 5). When only *trans* conformers were present, compound **10b** showed that only $18.3 \pm 0.3\%$ of the molecules inserted into the hydrophobic core of the membranes, while another $18.0 \pm 0.8\%$ were found at the interface of the membrane. The system with the *cis*-dominant (9:1) ratio showed the highest percentage of inserted molecules ($84.8 \pm 0.7\%$), while the *cis*-only system showed $31.1 \pm 0.9\%$ of the molecules had inserted, and a significant proportion of the molecules ($52.4 \pm 0.9\%$) were found at the interface of the membrane. In contrast, compound **10f** consistently exhibited superior membrane insertion across all conformer ratios. In the *trans*-only system, $81.0 \pm 0.9\%$ of the molecules inserted into the membrane and $19.0 \pm 0.9\%$ were found at the membrane interface. The *trans*-dominant (1:9) system showed $93.2 \pm 0.4\%$ insertion, while the *cis*-dominant (9:1) and *cis*-only (10:0) systems showed $98.3 \pm 0.3\%$ and 100.0% insertion, respectively. Interestingly, the equimolar (5:5) system exhibited fewer inserted molecules ($86.7 \pm 0.8\%$) compared to other systems, suggesting conformer-specific interactions that

	Insertion percentage (%)					
	<i>cis:trans</i> ratio					
	0:10	1:9	5:5	9:1	10:0	
10b	Inside	18.3	35.3	48.5	84.8	31.1
	Interface	18.0	30.4	20.5	15.2	52.4
	Outside	63.8	34.3	31.1	0	16.5
10f	Inside	81.0	93.2	86.7*	98.3	100
	Interface	19.0	6.8	13.3*	1.7	0
	Outside	0	0	0*	0	0



measured at time 175-200 ns to ensure the compounds were inserted for the membrane analysis.
*measured at time 140-154 ns

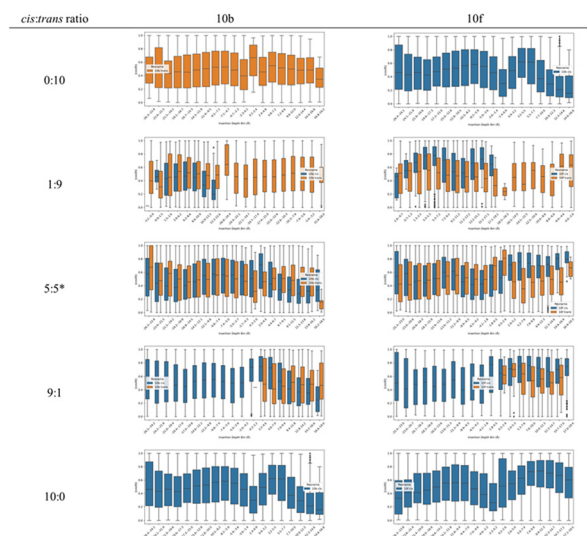
Fig. 6 Spatial distribution of membrane insertion for compound **10b** and **10f** across varying *cis:trans* conformer ratios. Data presented as mean. Inside (blue) = molecules embedded within membrane, interface (orange) = at the membrane-water interface (± 5 Å), outside (red) = in the aqueous phase.

affect membrane penetration dynamics as demonstrated in the insertion depth analysis.

These results indicate that the enhanced hydrophobic character of compound **10f** promotes consistent and deep membrane insertion, while compound **10b** with limited hydrophobic characteristics results in conformer-dependent and often significantly reduced membrane association.⁴⁴

To further investigate how the conformational state affects the interaction of the compound with the membrane, the orientation of the compound was evaluated as a function of insertion depth (Fig. 7). In all the simulated systems, the *cis* conformer of both compounds exhibited larger orientation values at shallow insertion depths (0–5 Å), with values approaching 1, indicative of the primary axis of the compound being parallel to the normal of the membrane during initial membrane engagement.^{45,46} At deeper insertion depths (10–20 Å), compound **10b** showed a decrease in orientation, suggesting a transition toward a more tilted orientation (or perpendicular) in relation to the normal vector of the membrane. The *trans* conformers also exhibited relatively large orientation values near the membrane interface, though this trend was less pronounced than in the *cis* conformers. In contrast, compound **10f** maintained large orientation values across all depths for both conformers, indicating that it remains vertical within the membrane irrespective of insertion depth.

This analysis revealed significant differences between the orientations taken by compounds **10b** and **10f** within the membrane (Fig. 8). For compound **10b**, the *cis* conformer showed a moderate increase in mean orientation with increasing *cis* content ($\cos(\theta) \sim 0.33$ to $\cos(\theta) \sim 0.48$), while the *trans* conformer remained relatively stable across most of



measured at time 175-200 ns to ensure the compounds were inserted for the membrane analysis.
*measured at time 140-154 ns for 10f

Fig. 7 Molecular orientation as a function of membrane insertion depth for compounds **10b** and **10f** across varying *cis:trans* conformer ratios. Orientation values approaching 1.0 indicate upright molecular alignment, while values near 0 suggest tilted or horizontal orientations. Error bars represent SEM.



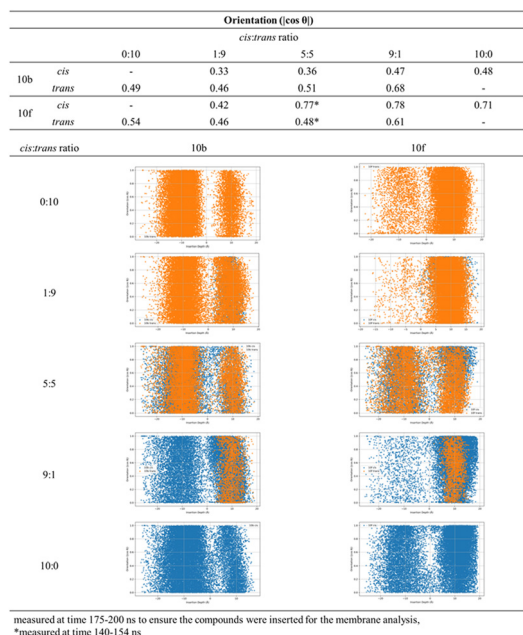


Fig. 8 Molecular orientation analysis showing mean orientation values ($\langle \cos \theta \rangle$) for compounds **10b** and **10f** across *cis:trans* conformer ratios.

the *cis:trans* ratios ($\cos(\theta) \sim 0.46$ – 0.51) but showed a notable increase in orientation in the systems with large *cis* ratios ($\cos(\theta) \sim 0.68$). Compound **10f** demonstrated markedly larger orientation values, with the *cis* conformer maintaining a consistently more tilted orientation ($\cos(\theta) \sim 0.42$ – 0.78) and the *trans* conformer became less tilted with decreasing *trans* content ($\cos(\theta) \sim 0.46$ – 0.61).

The differential antibacterial activity between compounds **10b** and **10f** correlates with their membrane insertion and orientation profiles. Compound **10f** demonstrated up to 32-fold increase in antibacterial efficacy upon irradiation, corresponding to the *cis*-dominant conditions. This enhanced activity aligns with the results from the molecular dynamics simulations showing optimal membrane insertion (98.3% at 9:1 ratio, 100% at 10:0 ratio) and superior orientational stability (0.78 *cis* orientation) when most of the molecules were in a *cis* conformation. In contrast, compound **10b** showed reduced antibacterial activity upon irradiation and showed only a modest reduction in potency, consistent with its limited and variable membrane insertion capabilities (maximum 84.8% at 9:1, only 31.1% at 10:0) and lower orientational alignment (maximum 0.48 for *cis* conformer).

The mechanistic basis for this structure–activity relationship lies in the membrane disruption requirements for antibacterial efficacy. Effective membrane disruption requires both deep membrane insertion and stable molecular orientation to create sufficient perturbation of the lipid bilayer integrity.^{47,48} Compound **10f** achieved these critical parameters specifically in *cis*-dominant conditions, where high insertion percentages combined with organised spatial distribution and optimal molecular alignment created the necessary membrane destabilization for bacterial cell death.

Compound **10b**, despite showing some membrane insertion and notable antibacterial activity in its *trans*-dominant state, lacked the consistent deep insertion and orientational stability required for effective membrane disruption. The superior hydrophobic character of compound **10f** enables the sustained membrane integration necessary for antimicrobial mechanism of action, while compound **10b** remains primarily at the interface without sufficient membrane disruption capacity to translate conformational changes into pronounced differences in antibacterial activity upon irradiation.

Conclusions

This study demonstrates that the antibacterial activity of amphiphilic lipids can be modulated by light through controlled photoisomerisation of azobenzene cores. The synthesised photoswitchable amphiphilic lipids (PALs) exhibit clear, chain-length-dependent responses to irradiation, with short-chain derivatives losing potency upon UV exposure, whereas longer-chain analogues become markedly more active in their *cis*-enriched states. Molecular dynamics simulations reveal that these changes arise from light-dependent differences in membrane insertion depth and molecular orientation, providing a mechanistic explanation for the observed photomodulation. Together, these findings show that reversible structural changes in lipid amphiphiles can translate into tunable antibacterial outcomes, establishing a rational framework for designing light-responsive membrane-active agents. Beyond their antibacterial potential, the PALs offer a model system for studying how molecular conformation governs membrane interactions, with implications for broader applications of photochemical control in chemical biology, pharmacology and medicinal chemistry.

Author contributions

G. F. S. F. and S.-H. K. performed the synthesis and microbiological evaluation of PALs and wrote of the manuscript; C. K. H., J. F.-P., J. R. performed the microbiology studies; S.-H. K. and C. D. L. performed the MD studies; A. J. M. and J. M. S. contributed to the supervision, conceptualization and design of the work; D. C. conceived and designed the project, contributed to the overall supervision of the team, and wrote the manuscript. All authors contributed to the preparation of this manuscript.

Conflicts of interest

There are no conflicts to declare.

Data availability

The data supporting this article, including synthetic procedures, compound characterisation data, UV-vis and NMR photoisomerisation studies, antibacterial assays, and molecular dynamics simulation methods, are available in the supplementary information (SI).



Supplementary information is available. See DOI: <https://doi.org/10.1039/d6md00096g>.

Acknowledgements

For G. F. S. F. and D. C. this project has received funding from the European Union's Horizon 2020 research and innovation programme under the Marie Skłodowska-Curie grant agreement No. 101027065. We are grateful to the UK Materials and Molecular Modelling Hub for computational resources, which is partially funded by EPSRC (EP/T022213/1, EP/W032260/1 and EP/P020194/1). We also appreciate the King's Computational Research, Engineering and Technology Environment (CREATE) at King's College London for providing us access to computational resources.⁴⁹ UKHSA Grant in Aid funding for the Open Innovation Platform (project 113361). SHK and AJM gratefully acknowledge University of London for the CW Maplethorpe Fellowship to SHK.

Notes and references

- J. G. Hurdle, A. J. O'Neill, I. Chopra and R. E. Lee, Targeting Bacterial Membrane Function: An Underexploited Mechanism for Treating Persistent Infections, *Nat. Rev. Microbiol.*, 2011, **9**(1), 62–75, DOI: [10.1038/nrmicro2474](https://doi.org/10.1038/nrmicro2474).
- R. M. Epanand, C. Walker, R. F. Epanand and N. A. Magarvey, Molecular Mechanisms of Membrane Targeting Antibiotics, *Biochim. Biophys. Acta, Biomembr.*, 2016, **1858**(5), 980–987, DOI: [10.1016/j.bbmem.2015.10.018](https://doi.org/10.1016/j.bbmem.2015.10.018).
- M. Rohde, The Gram-Positive Bacterial Cell Wall, *Microbiol. Spectrum*, 2019, **7**(3), DOI: [10.1128/microbiolspec.GPP3-0044-2018](https://doi.org/10.1128/microbiolspec.GPP3-0044-2018).
- M.-P. Mingeot-Leclercq and J.-L. Décout, Bacterial Lipid Membranes as Promising Targets to Fight Antimicrobial Resistance, Molecular Foundations and Illustration through the Renewal of Aminoglycoside Antibiotics and Emergence of Amphiphilic Aminoglycosides, *MedChemComm*, 2016, **7**(4), 586–611, DOI: [10.1039/C5MD00503E](https://doi.org/10.1039/C5MD00503E).
- D. Mehta, V. Saini, B. Aggarwal, A. Khan and A. Bajaj, Unlocking the Bacterial Membrane as a Therapeutic Target for Next-Generation Antimicrobial Amphiphiles, *Mol. Aspects Med.*, 2021, **81**, 100999, DOI: [10.1016/j.mam.2021.100999](https://doi.org/10.1016/j.mam.2021.100999).
- S.-H. Kim, C. K. Hind, G. F. S. Fernandes, J. Wu, D. Semenya, M. Clifford, C. Marsh, S. Anselmi, A. J. Mason, K. D. Bruce, J. M. Sutton and D. Castagnolo, Development of Novel Membrane Disrupting Lipoguanidine Compounds Sensitizing Gram-Negative Bacteria to Antibiotics, *ACS Med. Chem. Lett.*, 2024, **15**(2), 239–249, DOI: [10.1021/acsmmedchemlett.3c00460](https://doi.org/10.1021/acsmmedchemlett.3c00460).
- S. Li, M. Wang, S. Chen, M. Ampomah-Wireko, C. Gao, Z. Xia, L. Nininahazwe, S. Qin and E. Zhang, Development of Biaromatic Core-Linked Antimicrobial Peptide Mimics: Substituent Position Significantly Affects Antibacterial Activity and Hemolytic Toxicity, *Eur. J. Med. Chem.*, 2023, **247**, 115029, DOI: [10.1016/j.ejmech.2022.115029](https://doi.org/10.1016/j.ejmech.2022.115029).
- W. Cheng, T. Xu, L. Cui, Z. Xue, J. Liu, R. Yang, S. Qin and Y. Guo, Discovery of Amphiphilic Xanthohumol Derivatives as Membrane-Targeting Antimicrobials against Methicillin-Resistant Staphylococcus Aureus, *J. Med. Chem.*, 2023, **66**(1), 962–975, DOI: [10.1021/acs.jmedchem.2c01793](https://doi.org/10.1021/acs.jmedchem.2c01793).
- B. Findlay, G. G. Zhanel and F. Schweizer, Cationic Amphiphiles, a New Generation of Antimicrobials Inspired by the Natural Antimicrobial Peptide Scaffold, *Antimicrob. Agents Chemother.*, 2010, **54**(10), 4049–4058, DOI: [10.1128/AAC.00530-10](https://doi.org/10.1128/AAC.00530-10).
- M. Tischer, G. Pradel, K. Ohlsen and U. Holzgrabe, Quaternary Ammonium Salts and Their Antimicrobial Potential: Targets or Nonspecific Interactions?, *ChemMedChem*, 2012, **7**(1), 22–31, DOI: [10.1002/cmdc.201100404](https://doi.org/10.1002/cmdc.201100404).
- D. Kwaśniewska, Y.-L. Chen and D. Wiczorek, Biological Activity of Quaternary Ammonium Salts and Their Derivatives, *Pathogens*, 2020, **9**(6), 459, DOI: [10.3390/pathogens9060459](https://doi.org/10.3390/pathogens9060459).
- S. L. Regen, Membrane-Disrupting Molecules as Therapeutic Agents: A Cautionary Note, *JACS Au*, 2021, **1**(1), 3–7, DOI: [10.1021/jacsau.0c00037](https://doi.org/10.1021/jacsau.0c00037).
- W. A. Velema, W. Szymanski and B. L. Feringa, Photopharmacology: Beyond Proof of Principle, *J. Am. Chem. Soc.*, 2014, **136**(6), 2178–2191, DOI: [10.1021/ja413063e](https://doi.org/10.1021/ja413063e).
- M. J. Fuchter, On the Promise of Photopharmacology Using Photoswitches: A Medicinal Chemist's Perspective, *J. Med. Chem.*, 2020, **63**(20), 11436–11447, DOI: [10.1021/acs.jmedchem.0c00629](https://doi.org/10.1021/acs.jmedchem.0c00629).
- P. Kobauri, F. J. Dekker, W. Szymanski and B. L. Feringa, Rational Design in Photopharmacology with Molecular Photoswitches, *Angew. Chem., Int. Ed.*, 2023, **62**(30), e202300681, DOI: [10.1002/anie.202300681](https://doi.org/10.1002/anie.202300681).
- F. A. Jerca, V. V. Jerca and R. Hoogenboom, Advances and Opportunities in the Exciting World of Azobenzenes, *Nat. Rev. Chem.*, 2021, **6**(1), 51–69, DOI: [10.1038/s41570-021-00334-w](https://doi.org/10.1038/s41570-021-00334-w).
- E. Merino, Synthesis of Azobenzenes: The Coloured Pieces of Molecular Materials, *Chem. Soc. Rev.*, 2011, **40**(7), 3835–3853, DOI: [10.1039/c0cs00183j](https://doi.org/10.1039/c0cs00183j).
- T. C. De Souza-Guerreiro, G. Bondelli, I. Grobas, S. Donini, V. Sesti, C. Bertarelli, G. Lanzani, M. Asally and G. M. Paternò, Membrane Targeted Azobenzene Drives Optical Modulation of Bacterial Membrane Potential, *Adv. Sci.*, 2023, **10**(8), 2205007, DOI: [10.1002/advs.202205007](https://doi.org/10.1002/advs.202205007).
- Y. Zhang, J. Deng, H. Tian, H. Qi, T. Xiong, S. Lin, Y. Dong, L. Luo, D. Wu, K. Zhang, M. Ji, T. Du, L. Sheng, X. Chen and H. Xu, Design, Synthesis, and Bioevaluation of Novel Reversibly Photoswitchable PI3K Inhibitors Based on Phenylazopyridine Derivatives toward Light-Controlled Cancer Treatment, *J. Med. Chem.*, 2024, **67**, 3504–3519, DOI: [10.1021/acs.jmedchem.3c01864](https://doi.org/10.1021/acs.jmedchem.3c01864).
- A. Müller-Deku, J. C. M. Meiring, K. Loy, Y. Kraus, C. Heise, R. Bingham, K. I. Jansen, X. Qu, F. Bartolini, L. C. Kapitein, A. Akhmanova, J. Ahlfeld, D. Trauner and O. Thorn-Seshold, Photoswitchable Paclitaxel-Based



- Microtubule Stabilisers Allow Optical Control over the Microtubule Cytoskeleton, *Nat. Commun.*, 2020, **11**(1), 4640, DOI: [10.1038/s41467-020-18389-6](https://doi.org/10.1038/s41467-020-18389-6).
- 21 M. Borowiak, W. Nahaboo, M. Reynders, K. Nekolla, P. Jalinet, J. Hasserodt, M. Rehberg, M. Delattre, S. Zahler, A. Vollmar, D. Trauner and O. Thorn-Seshold, Photoswitchable Inhibitors of Microtubule Dynamics Optically Control Mitosis and Cell Death, *Cell*, 2015, **162**(2), 403–411, DOI: [10.1016/j.cell.2015.06.049](https://doi.org/10.1016/j.cell.2015.06.049).
- 22 D. M. Barber, S.-A. Liu, K. Gottschling, M. Sumser, M. Hollmann and D. Trauner, Optical Control of AMPA Receptors Using a Photoswitchable Quinoxaline-2,3-Dione Antagonist, *Chem. Sci.*, 2017, **8**(1), 611–615, DOI: [10.1039/C6SC01621A](https://doi.org/10.1039/C6SC01621A).
- 23 M. Banghart, K. Borges, E. Isacoff, D. Trauner and R. H. Kramer, Light-Activated Ion Channels for Remote Control of Neuronal Firing, *Nat. Neurosci.*, 2004, **7**(12), 1381–1386, DOI: [10.1038/nn1356](https://doi.org/10.1038/nn1356).
- 24 S. A. Reis, B. Ghosh, J. A. Hendricks, D. M. Szantai-Kis, L. Türk, K. N. Ross, J. Lamb, W. Read-Button, B. Zheng, H. Wang, C. Salthouse, S. J. Haggarty and R. Mazitschek, Light-Controlled Modulation of Gene Expression by Chemical Optoepigenetic Probes, *Nat. Chem. Biol.*, 2016, **12**(5), 317–323, DOI: [10.1038/nchembio.2042](https://doi.org/10.1038/nchembio.2042).
- 25 L. Josa-Culleré and A. Llebaria, Visible-Light-Controlled Histone Deacetylase Inhibitors for Targeted Cancer Therapy, *J. Med. Chem.*, 2023, **66**(3), 1909–1927, DOI: [10.1021/acs.jmedchem.2c01713](https://doi.org/10.1021/acs.jmedchem.2c01713).
- 26 D. Kolarski, C. Miró-Vinyals, A. Sugiyama, A. Srivastava, D. Ono, Y. Nagai, M. Iida, K. Itami, F. Tama, W. Szymanski, T. Hirota and B. L. Feringa, Reversible Modulation of Circadian Time with Chronopharmacology, *Nat. Commun.*, 2021, **12**(1), 3164, DOI: [10.1038/s41467-021-23301-x](https://doi.org/10.1038/s41467-021-23301-x).
- 27 Y.-H. Tsai, S. Essig, J. R. James, K. Lang and J. W. Chin, Selective, Rapid and Optically Switchable Regulation of Protein Function in Live Mammalian Cells, *Nat. Chem.*, 2015, **7**(7), 554–561, DOI: [10.1038/nchem.2253](https://doi.org/10.1038/nchem.2253).
- 28 A. Magni, G. Bondelli, G. M. Paternò, S. Sardar, V. Sesti, C. D'Andrea, C. Bertarelli and G. Lanzani, Azobenzene Photoisomerization Probes Cell Membrane Viscosity, *Phys. Chem. Chem. Phys.*, 2022, **24**(15), 8716–8723, DOI: [10.1039/D1CP05881A](https://doi.org/10.1039/D1CP05881A).
- 29 W. A. Velema, J. P. van der Berg, M. J. Hansen, W. Szymanski, A. J. M. Driessen and B. L. Feringa, Optical Control of Antibacterial Activity, *Nat. Chem.*, 2013, **5**(11), 924–928, DOI: [10.1038/nchem.1750](https://doi.org/10.1038/nchem.1750).
- 30 Y. Hu, W. Zou, V. Julita, R. Ramanathan, R. F. Tabor, R. Nixon-Luke, G. Bryant, V. Bansal and B. L. Wilkinson, Photomodulation of Bacterial Growth and Biofilm Formation Using Carbohydrate-Based Surfactants, *Chem. Sci.*, 2016, **7**(11), 6628–6634, DOI: [10.1039/C6SC03020C](https://doi.org/10.1039/C6SC03020C).
- 31 A. Franche, A. Fayeulle, L. Lins, M. Billamboz, I. Pezron, M. Deleu and E. Léonard, Amphiphilic Azobenzenes: Antibacterial Activities and Biophysical Investigation of Their Interaction with Bacterial Membrane Lipids, *Bioorg. Chem.*, 2020, **94**, 103399, DOI: [10.1016/j.bioorg.2019.103399](https://doi.org/10.1016/j.bioorg.2019.103399).
- 32 E. Chevallier, A. Mamane, H. A. Stone, C. Tribet, F. Lequeux and C. Monteux, Pumping-out Photo-Surfactants from an Air–Water Interface Using Light, *Soft Matter*, 2011, **7**(17), 7866–7874, DOI: [10.1039/c1sm05378g](https://doi.org/10.1039/c1sm05378g).
- 33 Z. E. A. Toles, A. Wu, C. A. Sanchez, M. E. Michaud, L. M. Thierer, W. M. Wuest and K. P. C. Minbiole, Double BAC and Triple BAC: A Systematic Analysis of the Disinfectant Properties of Multicationic Derivatives of Benzalkonium Chloride (BAC), *ChemMedChem*, 2023, **18**(10), e202300018, DOI: [10.1002/cmdc.202300018](https://doi.org/10.1002/cmdc.202300018).
- 34 M. A. Seferyan, E. A. Saverina, N. A. Frolov, E. V. Detusheva, O. A. Kamanina, V. A. Arlyapov, I. I. Ostashevskaya, V. P. Ananikov and A. N. Vereshchagin, Multicationic Quaternary Ammonium Compounds: A Framework for Combating Bacterial Resistance, *ACS Infect. Dis.*, 2023, **9**(6), 1206–1220, DOI: [10.1021/acsinfecdis.2c00546](https://doi.org/10.1021/acsinfecdis.2c00546).
- 35 S. Buffet-Bataillon, P. Tattevin, M. Bonnaure-Mallet and A. Jolivet-Gougeon, Emergence of Resistance to Antibacterial Agents: The Role of Quaternary Ammonium Compounds—a Critical Review, *Int. J. Antimicrob. Agents*, 2012, **39**(5), 381–389, DOI: [10.1016/j.ijantimicag.2012.01.011](https://doi.org/10.1016/j.ijantimicag.2012.01.011).
- 36 F. Devínský, A. Kopecka-Leitmanová, F. Šeršeň and P. Balgavý, Cut-off Effect in Antimicrobial Activity and in Membrane Perturbation Efficiency of the Homologous Series of N,N-Dimethylalkylamine Oxides, *J. Pharm. Pharmacol.*, 2011, **42**(11), 790–794, DOI: [10.1111/j.2042-7158.1990.tb07022.x](https://doi.org/10.1111/j.2042-7158.1990.tb07022.x).
- 37 J. Łuczak, C. Jungnickel, I. Łącka, S. Stolte and J. Hupka, Antimicrobial and Surface Activity of 1-Alkyl-3-Methylimidazolium Derivatives, *Green Chem.*, 2010, **12**(4), 593–601, DOI: [10.1039/b921805j](https://doi.org/10.1039/b921805j).
- 38 B. J. Denny, L. Novotny, P. W. J. West, M. Blesova and J. Zamocka, Antimicrobial Activity of a Series of 1-Alkyl-2-(4-Pyridyl)Pyridinium Bromides against Gram-Positive and Gram-Negative Bacteria, *Med. Princ. Pract.*, 2005, **14**(6), 377–381, DOI: [10.1159/000088108](https://doi.org/10.1159/000088108).
- 39 C. R. Birnie, D. Malamud and R. L. Schnaare, Antimicrobial Evaluation of N-Alkyl Betaines and N-Alkyl-N,N-Dimethylamine Oxides with Variations in Chain Length, *Antimicrob. Agents Chemother.*, 2000, **44**(9), 2514–2517, DOI: [10.1128/AAC.44.9.2514-2517.2000](https://doi.org/10.1128/AAC.44.9.2514-2517.2000).
- 40 H. K. Ganguly and G. Basu, Conformational Landscape of Substituted Prolines, *Biophys. Rev.*, 2020, **12**(1), 25–39, DOI: [10.1007/s12551-020-00621-8](https://doi.org/10.1007/s12551-020-00621-8).
- 41 A. Altis, P. H. Nguyen, R. Hegger and G. Stock, Dihedral Angle Principal Component Analysis of Molecular Dynamics Simulations, *J. Chem. Phys.*, 2007, **126**(24), 244111, DOI: [10.1063/1.2746330](https://doi.org/10.1063/1.2746330).
- 42 G. S. Lim, S. Jaenicke and M. Klähn, How the Spontaneous Insertion of Amphiphilic Imidazolium-Based Cations Changes Biological Membranes: A Molecular Simulation Study, *Phys. Chem. Chem. Phys.*, 2015, **17**(43), 29171–29183, DOI: [10.1039/c5cp04806k](https://doi.org/10.1039/c5cp04806k).
- 43 I. Kabelka and R. Vácha, Optimal Hydrophobicity and Reorientation of Amphiphilic Peptides Translocating



- through Membrane, *Biophys. J.*, 2018, **115**(6), 1045–1054, DOI: [10.1016/j.bpj.2018.08.012](https://doi.org/10.1016/j.bpj.2018.08.012).
- 44 A. Jayawardena, A. Hung, G. Qiao and E. Hajizadeh, Molecular Dynamics Simulation of the Interaction of Lipidated Structurally Nano Engineered Antimicrobial Peptide Polymers with Bacterial Cell Membrane, *J. Phys. Chem. B*, 2025, **129**(37), 9382–9393, DOI: [10.1021/acs.jpcc.5c02067](https://doi.org/10.1021/acs.jpcc.5c02067).
- 45 S. K. Kandasamy and R. G. Larson, Molecular Dynamics Simulations of Model Trans-Membrane Peptides in Lipid Bilayers: A Systematic Investigation of Hydrophobic Mismatch, *Biophys. J.*, 2006, **90**(7), 2326–2343, DOI: [10.1529/biophysj.105.073395](https://doi.org/10.1529/biophysj.105.073395).
- 46 S. Esteban-Martín and J. Salgado, The Dynamic Orientation of Membrane-Bound Peptides: Bridging Simulations and Experiments, *Biophys. J.*, 2007, **93**, 4278–4288, DOI: [10.1529/biophysj.107.115428](https://doi.org/10.1529/biophysj.107.115428).
- 47 F. R. Fields, G. Manzo, C. K. Hind, J. Janardhanan, I. P. Foik, P. D. Carmo Silva, R. D. Balsara, M. Clifford, H. M. Vu, J. N. Ross, V. R. Kalwajtys, A. J. Gonzalez, T. T. Bui, V. A. Ploplis, F. J. Castellino, A. Siryaporn, M. Chang, J. M. Sutton, S. Lee and A. J. Mason, Synthetic Antimicrobial Peptide Tuning Permits Membrane Disruption and Interpeptide Synergy, *ACS Pharmacol. Transl. Sci.*, 2020, **3**(2), 418–424, DOI: [10.1021/acsptsci.0c00001](https://doi.org/10.1021/acsptsci.0c00001).
- 48 A. Hollmann, M. Martínez, M. E. Noguera, E. A. Disalvo and J. Santos, Antimicrobial Peptides: Interaction With Model and Biological Membranes and Synergism With Chemical Antibiotics, *Front. Chem.*, 2018, **6**, 204, DOI: [10.3389/fchem.2018.00204](https://doi.org/10.3389/fchem.2018.00204).
- 49 e-Research King's Computational Research, Engineering and Technology Environment (CREATE), 2025, <https://docs.er.kcl.ac.uk/>.

